IEEE Photonics Journal
An IEEE Photonics Society Publication

Open Access

Numerical Simulation and Experiment on Optical Packet Header Recognition Utilizing Reservoir Computing Based on Optoelectronic Feedback

Volume 9, Number 1, February 2017

Jie Qin
Qingchun Zhao
Hongxi Yin
Yu Jin
Chang Liu

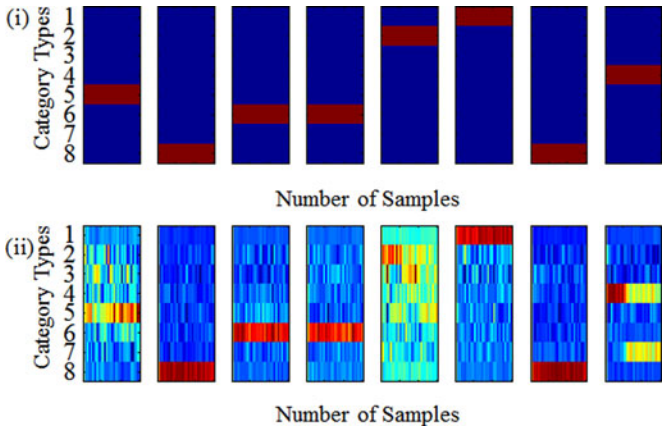

DOI: 10.1109/JPHOT.2017.2658028
1943-0655

IEEE photonics SOCIETY

IEEE

Numerical Simulation and Experiment on Optical Packet Header Recognition Utilizing Reservoir Computing Based on Optoelectronic Feedback

Jie Qin,[1] Qingchun Zhao,[1,2] Hongxi Yin,[1] Yu Jin,[1] and Chang Liu[1]

[1]School of Information and Communication Engineering, Dalian University of Technology, Dalian 116023, China
[2]School of Computer and Communication Engineering, Northeastern University at Qinhuangdao, Qinhuangdao 066004, China

DOI:10.1109/JPHOT.2017.2658028

Manuscript received January 5, 2017; revised January 17, 2017; accepted January 19, 2017. Date of publication January 25, 2017; date of current version February 14, 2017. This work was supported in part by the National Natural Science Foundation of China under Grant 61071123 and Grant 61602099, in part by the Natural Science Foundation of Hebei province of China under Grant F2016501169, in part by the colleges and universities in Hebei province Science and Technology Research Project under Grant QN2015312, and in part by the Fundamental Research Funds for the Central Universities under Grant N152303003. Corresponding author: H. Yin (e-mail: hxyin@dlut.edu.cn).

Abstract: An optoelectronic feedback reservoir computing (RC) system that can identify optical packet headers for an optical packet switching (OPS) network is proposed and implemented by the numerical simulation and the experiment in this paper. First, a simulation system of optical packet header recognition based on the optoelectronic feedback RC is established through optimizing its parameters. It is shown that the optoelectronic feedback RC system can correctly identify optical packet headers with lengths from 3 bits to 32 bits and that the recognition word-error rate (WER) is 0. Then, an experiment system consistent with the optimal simulation system is set up, whose WER for the 3-bit header recognition is only 1.25%. The experimental results also indicate that the bias voltage of the Mach–Zehnder modulator (MZM) has a significant impact on recognition results. When the RC system is in the critical state between the multiple-period oscillation and the chaos, the maximal Lyapunov exponent is slightly larger than 0, and the recognition normalized root-mean-square error (NRMSE) reaches its minimal value.

Index Terms: Reservoir computing (RC), chaos, optical packet header recognition, optoelectronic feedback.

1. Introduction

With the rapid development of modern society, the massive growth of data greatly promotes the development of communications technologies. The optical communication network has many advantages such as the high bandwidth, the large capacity, the low loss, etc., so that it plays an irreplaceable role in the wired communication system. Compared with the existing optical circuit switching (OCS) network, the optical packet switching (OPS) network has the greater potential for the high bandwidth utilization and the low power consumption [1]–[3]. An optical packet consists of an optical packet header and a payload, and the former contains the routing information and the

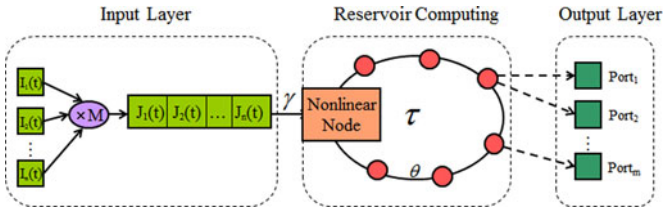

Fig. 1. Structure diagram of the single node reservoir computing for pattern recognition.

latter carries user's data. A router in an OPS network can extract headers, identify types of headers, process the routing information, and send the optical packet to a proper port [4], [5], that is, the identification of optical packet headers determines whether the routing information can be obtained correctly, which becomes one of key techniques of an OPS network.

During recent years, some literatures have focused the optical packet header recognition techniques. A scalable photonic-integrated architecture comprised of the cascaded SOA-based Mach-Zehnder interferometers was proposed for the all-optical packet header processing in [6]. A compensator utilizing the time-to-space conversion and the spatial two-dimensional correlation was proposed for the optical label recognition in [7]. However, these techniques have a critical disadvantage of low output contrast so that the extra optical devices is indispensable to compensate the output contrast. In addition to methods mentioned above, the optical-packet header processing through utilizing the optical neural network has become a new hotspot [8]–[11]. The reservoir computing with a single node is a new type of artificial neural network consisting of one nonlinear node and one delay line [37]–[39], whose hardware cost is significantly reduced in comparison with the traditional neural network [12]–[16]. As a single node RC, the optoelectronic feedback reservoir computing can be easily implemented by several optoelectronic devices [17]–[19]. With the quite simple training process on its output layer, the RC system can achieve different pattern recognitions and time series prediction tasks [20]–[22]. In addition, since the reservoir computing system contains many nonlinear states it can be employed as the analog computer to directly process analog signals without the digital quantization [23]–[25]. Overall, the optoelectronic feedback RC has more powerful information processing ability and less system complexity than a traditional neural network. Therefore, it can process a variety of high-speed optical signals under different application backgrounds [26]–[30].

In this paper, an optoelectronic feedback RC is applied to realize the task of the optical packet header identification for the OPS network. We numerically simulate the optoelectronic feedback RC to identify the optical packet headers with 3 bits, 16 bits, and 32 bits, respectively. Then we establish the experiment system consistent with the numerical simulation. Besides, the impact of system parameters such as a modulator bias voltage and a feedback optical power on recognition results is analyzed in detail.

2. Principle of the Optoelectronic Feedback RC

Fig. 1 shows the structure diagram of the single node reservoir computing that can identify the optical packet headers and map them to corresponding routing ports after being trained. $I_i(t)$ represents the n types of packet headers and then multiply with the preprocessing mask M to construct the serial input signal $J_i(t)$. After being amplified γ times, the input signal $J_i(t)$ is applied to the nonlinear node and transmitted in the feedback delay loop. In the RC's output layer, the nonlinear mapped signal is trained and tested utilizing the ridge regression algorithm [31], [32].

The block diagram of the optical packet header recognition utilizing the photoelectric feedback reservoir computing is shown in Fig. 2. The continuous-wave light generated by a laser diode (LD) turns to the nonlinear oscillation on account of the reservoir that is composed of a Mach-Zehnder modulator (MZM), an optical delay line (ODL), an optical coupler (OC), a variable optical attenuator (VOA), a photodiode (PD), an electronic amplifier (AMP), and a low-pass filter (LPF). Optical packet

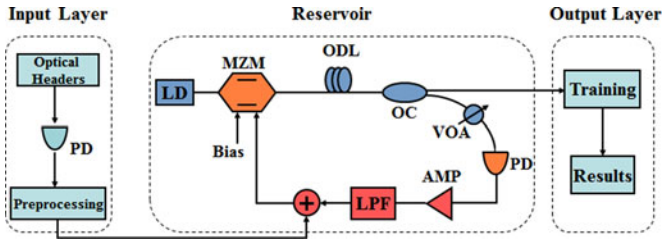

Fig. 2. Structure diagram of the photoelectric feedback RC for identifying the optical headers. LD: laser diode, MZM: Mach-Zehnder modulator, ODL: optical delay line, OC: optical coupler, VOA: variable optical attenuator, PD: photodiode, AMP: amplifier, LPF: low-pass filter.

headers after being optoelectric conversion are added with the feedback electric signals and are fed into the MZM's RF port. The nonlinearity of the MZM can be changed by loading different voltages at the bias port. The OC divides the RC's output signal into two parts, where one part is fed back and another part is sent to the output layer for the training and testing recognition results.

The dynamic behavior of the optoelectric feedback system is represented as the following equation [33]–[36]:

$$\frac{1}{\theta}\int_{t_0}^{t} x(\varepsilon)\,\mathrm{d}\varepsilon + x(t) + \tau\frac{\mathrm{d}x(t)}{\mathrm{d}t} = \beta\cos^2\left[x(t-T)+\phi\right] \tag{1}$$

where $x(t) = \pi V(t)/2\,V_\pi$ is the normalized bias voltage of MZM, $V(t)$ represents the amplifier's output voltage, and V_π is the half-wave voltage of the MZM. $\theta = 1/(2\,\pi f_L)$ and $\tau = 1/(2\,\pi f_H)$ represent the low-frequency cutoff characteristic time and the high-frequency cutoff characteristic time, respectively, where f_L and f_H are cutoff frequencies of the low-frequency and high-frequency for the RC system. In addition, β is the feedback coefficient, T is the feedback delay time and ϕ is the offset phase of the MZM. To solve Eq. (1), we can introduce variable $y = \int_{t_0}^{t} x(\varepsilon)\mathrm{d}\varepsilon$ to replace the integral term so that the Eq. (1) can be reduced to

$$\begin{cases} x' = -x/\tau - y/(\tau\theta) + \beta\cos^2\left[x(t-T)+\phi\right]/\tau \\ y' = x. \end{cases} \tag{2}$$

If the input signal $J(t)$ is considered, the equation set becomes

$$\begin{cases} x' = -x/\tau - y/(\tau\theta) + \beta\cos^2\left[x(t-T)+J(t)+\phi\right]/\tau \\ y' = x. \end{cases} \tag{3}$$

In the numerical simulation, the parameters are chosen as follows according to [17], [19], [40]: $\tau = 19.89$ ps, $\theta = 51.34$ ps, $T = 2.5$ ns, $\phi = -\pi/4$, $V_\pi = 5$ V. The feedback coefficient β is a significant parameter that can affect the nonlinear state of the system and the result of identification. After the RC's internal state vector x trained, the connection weights matrix W of the output layer is fixed and then, we can get the RC's output vector $\hat{y} = W \cdot x$. To evaluate the identification results, we calculate the normalized root mean square error (NRMSE) and the word error rate (WER) as expressed by Eq. (4) and Eq. (5) to indicate the accuracy and reliability of the identification. In Eq. (4), $\hat{y}(t)$ and $y(t)$ represent the RC's actual output and the target output at time t respectively, while n is the length of discrete data. In Eq. (5), N_{all} is the total number of the optical headers, while $N_{correct}$ is the number of correctly identified headers (we define one header as a "word"). The NRMSE represents the deviation between the target output and the actual output whose acceptable value is less than 0.2 according to [22], [29], and [30] for a good recognition result. The WER indicates the reliability of

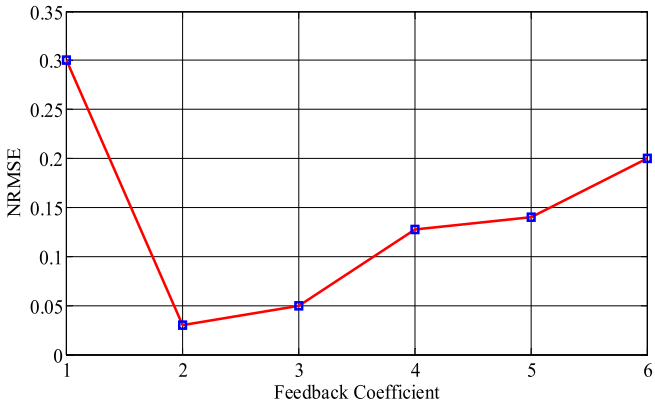

Fig. 3. Relationship between the NRMSE and the feedback coefficient.

the optical packet switching networks. Its value should be less than 0.02.

$$NRMSE = \sqrt{\frac{\left\langle (\hat{y}(t) - y(t))^2 \right\rangle}{\left\langle (y(t) - \langle y(t) \rangle_t)^2 \right\rangle_t}} = \sqrt{\frac{\frac{1}{n}\sum_{t=1}^{n} (\hat{y}(t) - y(t))^2}{\frac{1}{n}\sum_{t=1}^{n} \left(y(t) - \frac{1}{n}\sum_{t=1}^{n} y(t)\right)^2}} \tag{4}$$

$$WER = \frac{N_{all} - N_{correct}}{N_{all}} \times 100\% \tag{5}$$

3. Simulation Results

To quickly find the optimal parameters of the simulation system, we choose the 3-bit optical packet header as the RC's input signal. Eight types of 3-bit headers (000∼111) are generated while each bit is sampled by 6 points to imitate the analog RC system. The bit rate for our simulation system is 10 Gbps. The total number of the optical packet headers is 80 (64 headers for training and 16 headers for testing). The virtual node number of the RC is 400 with the corresponding mask whose elements are randomly distributed ± 0.1 for the preprocessing.

The results of the optical packet header recognition under different feedback coefficients are shown in Fig. 3 whose NRMSE is firstly decreased and then increased. The optimal feedback coefficient β is 2 with the minimal NRMSE as 0.0352 and the minimal WER as 0. With the increase of β, the RC's state changes from the periodic oscillation state to the chaotic state and will be in the transient state when β equals to 2. In the transient state, the RC has an infinite dimensional space so the input signal is mapped to the higher dimensional space and becomes more linearly separable. This is why the RC can achieve the recognition tasks.

The recognition results of 8 types of optical packet headers matching with the 8 output ports are shown in Fig. 4. Different color lines represent different types of the optical packet headers. The target output of correct identification is $+1$ while the wrong identification is -1 oppositely. As seen from Fig. 4, all the headers can be mapped to the corresponding output ports correctly.

Optical packet headers often carry the white Gauss noise since there are the active optical devices such as lasers or optical amplifiers in an optical communication system. In our simulation, we set the signal-to-noise ratio (SNR) of the optical packet headers from 10 dB to 80 dB and the NRMSE curve of recognition is shown in Fig. 5. The optoelectronic feedback RC system will incorrectly identify the optical packet headers when the SNR is 10 dB. The corresponding NRMSE is 0.3361 and the WER is 3.75%, i.e., three among 80 optical headers can be identified incorrectly. When the SNR is above 20 dB, the NRMSE is lower than 0.15, and the WER is 0. These results indicate that the optoelectronic feedback RC could be applied to the OPS network in the matter of noise tolerance.

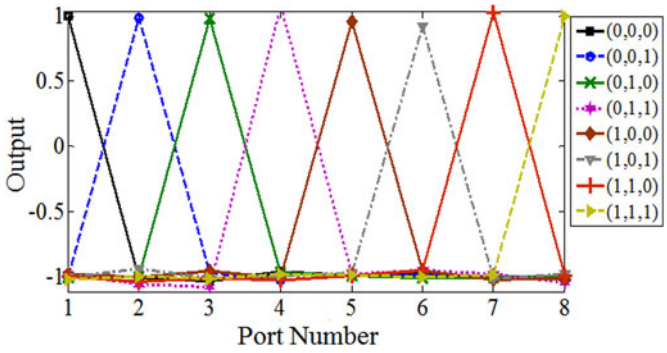

Fig. 4. Optical packet header (3 bits) recognition results, NRMSE = 0.0352, WER = 0.

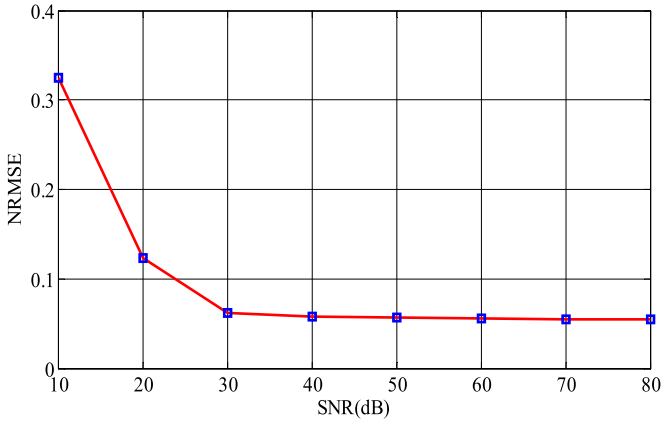

Fig. 5. Identification NRMSE with the variation of SNR.

The actual optical packet headers have different lengths and the router information is always a 2^n-bit long binary sequence, and therefore, the recognition for 8 types of packet headers with the length of 8 bits, 16 bits and 32 bits is implemented in our simulation. The optoelectronic feedback reservoir computing has good scalability that can identify various types of the optical packet headers with different lengths. While RC may be used in the high-speed optical packet switching networks as the backbone network with less types of routing information, we mainly focused on 8 types of the optical packet headers in the simulations. The corresponding recognition results are shown in Fig. 6(a)–(c) respectively. The NRMSE of each subfigure from the top to the bottom is 0.0374, 0.0389 and 0.0391 while all the recognition WER is 0. These results show that the optoelectronic feedback RC system can identify the optical packet headers with different lengths in different practical tasks for an OPS network.

4. Experimental Results

The structure diagram of the experimental system based on the optoelectronic feedback RC is shown in Fig. 7(a) and (b) is the photo of test bed. A distributed feedback Bragg (DFB, 1551.72 nm) laser generates continuous-wave light with the optical power of −3 dBm. Through the Erbium-doped fiber amplifier (EDFA1) and the variable optical attenuator (VOA1), the optical power is stable at 7 dBm. The polarization controller (PC1) before the Mach-Zehnder modulator (MZM, MXAN-LN-10) is arranged to adjust the polarization. The input electronic signal is changed to optical signal by the MZM. The optical signal is amplified to 7 dBm by EDFA2. The time delay for the feedback loop is 9.67 ns produced by a 2-meter long standard single-mode fiber (SSMF). Then,

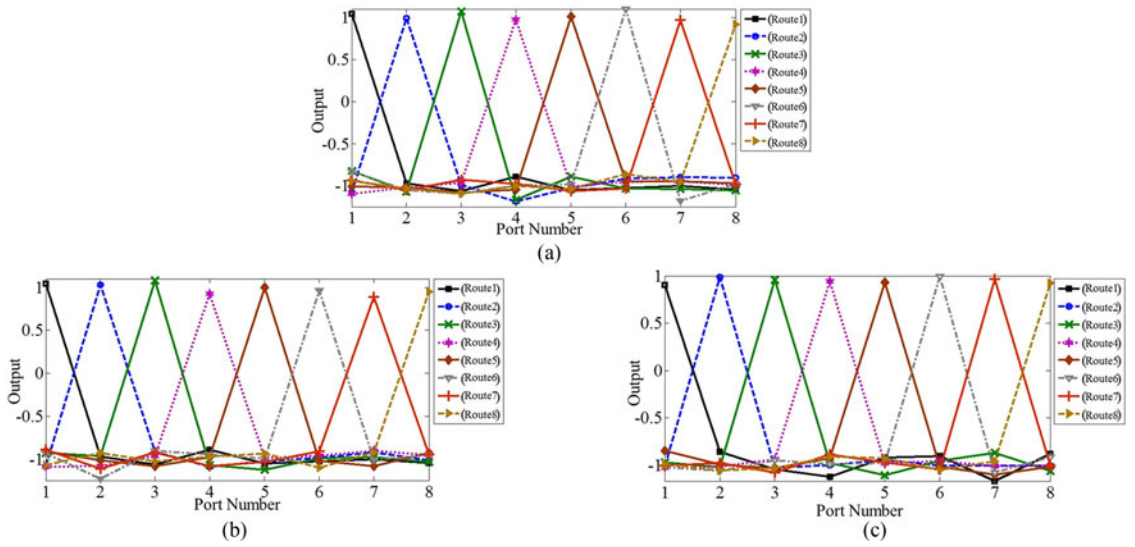

Fig. 6. Recognition results for optical packet headers with different lengths. (a) 8-bit header. (b) 16-bit header. (c) 32-bit header.

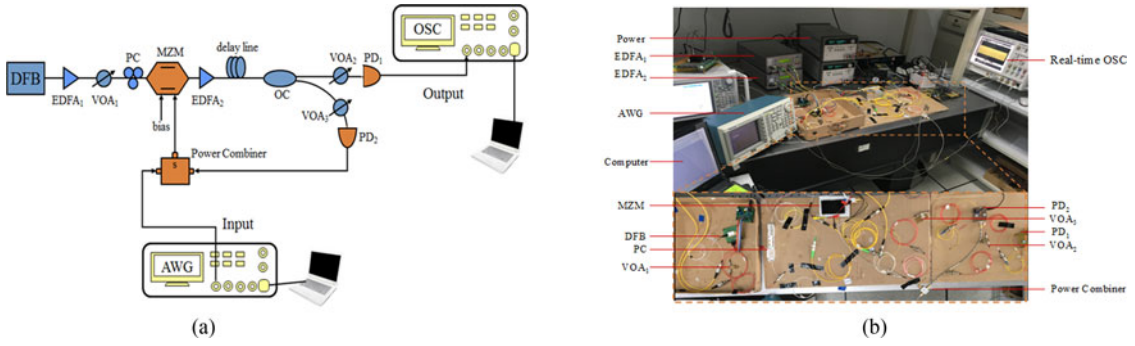

Fig. 7. Structure diagram and photo of the optical headers identification experiment. (a) Structure diagram of the experimental system. (b) Identification experiment. DFB: distributed feedback laser, MZM: Mach-Zehnder modulator, PC: polarization controller, VOA: variable optical attenuator, PD: photodiode, AWG: arbitrary waveform generator, OSC: oscilloscope, EDFA: Erbium-doped fiber amplifier.

the 50:50 optical coupler (OC) divides the light into two parts. One part is sent to the output layer of RC for training, and another part is fed back to the RF port of the MZM through the photodiode (PD2, DSC-R401HG-39) and the power combiner. The other input port of the power combiner is connected with the arbitrary waveform generator (AWG, Tektronix AFG 3101) that is controlled by a laptop so that different types of packet headers can be generated in our experiment. In our numerical simulations, we can set the bit rate as 10 Gbps to simulate the high speed OPS networks and operate on data at picosecond level. Limited by the laboratory equipments as the arbitrary waveform generator whose maximal bandwidth is 10 MHz and the digital storage oscilloscope whose maximal bandwidth is 4 GHz, we can only generate and analyze the low speed data and verify the feasibility of the recognition task using the proposed optoelectronic feedback reservoir computing. In the future, we will use high-speed FPGA boards to generate the optical packet headers and the preprocessing masks at ∼Gbps level in order not to be limited by the bandwidths of the AWG and OSC. Our compiling software is employed to generate the preprocessed 3-bit packet headers with a frequency of 10 MHz and the amplitude of 2 V. There are eight types of 3-bit packet headers at the input layer and each type contains ten repeated headers. The photodiode (PD1, DSC-R401HG-39) converts the light signal into the electric signal and sends it to the digital

storage oscilloscope (OSC, Agilent DSO90404A) that saves the output data for training and testing. The sampling rate of the OSC is 4 GSa/s. The virtual node number is 400. The preprocessing mask consists of 400 randomly distributed $+0.1$ and -0.1. We generated and recorded 80 sets of data with 64 sets for training and 16 sets for testing.

During the experiment, we adjust the parameters of the experimental devices according to the parameters used in the simulations. The typical parameters in the numerical simulations are τ, θ, T, ϕ, V_π, and β. τ is the high-frequency cutoff characteristic time of the optoelectronic feedback loop, while θ is the low-frequency cutoff characteristic time of the feedback loop. In our laboratory, we have no vector network analyzer, so the transfer function of the optoelectronic feedback loop is not experimentally obtained to calculate the two parameters τ and θ. The standard single-mode fiber (SSMF) whose refractive index as 1.45 is a 2-meter fiber jumper. Hence, the corresponding time delay is 9.67 ns in the experiment. The time delay in the simulation is 2.5 ns. The simulation time for a PC increases dramatically with the increasing time delay. 2.5 ns time delay is chosen according to reference [40]. ϕ is the offset phase of the MZM, which is not measured in the experiment. V_π is the half-wave voltage of the MZM. The half-wave voltage of the MZM we measured in the experiment is 6 V. In simulation, the normalized feedback coefficient β has typical values from 0 to 5, while in the experiment we adjust the optical power in the optoelectronic feedback loop by the variable optical attenuator (VOA3) to record the output waveform of the RC. For the simulation of the optoelectronic feedback loop, the normalized voltage that drives the MZM, i.e., $x(t)$ is usually concerned, which is a voltage variable. However, in the experiment, the optical power of the feedback loop is generally measured by an optical power meter, but the change trend for the optical power and the normalized voltage $x(t)$ with the variable parameters is consistent. The purpose of our simulations is to study the change trend in order to provide some information about the parameters adjustment in the experiment.

Adjusting the bias voltage of the MZM will change the nonlinearity of virtual nonlinear nodes and the output of the RC system as well. Fig. 8 indicates the different waveforms observed on the oscilloscope under different bias voltages. When the bias voltage is 0, there is a constant output as shown in Fig. 8(a). Increasing the bias voltage, the period oscillations of different frequencies are obserived as shown in Fig. 8(b) and (c). It is worth noting that when the bias voltage is between 3.9 V and 4 V, the waveform is in a transient state between the period oscillation and chaos. While bias voltage is above 4 V, the waveform turns to chaos as shown in Fig. 8(d).

Different outputs of the RC indicate different nonlinear states. Here the maximal Lyapunov exponent (MLE) is utilized to determine whether an experimental time trace is chaos or not. The output data are recorded by the OSC. The MLE is calculated by a PC according to the steps of [41]–[43]. The phase space reconstruction is realized according to the experimental time trace. Note that the time delay τ and the embedding dimension m are calculated by the CC algorithm. For a more detailed calculation, see [41, App. 3]. If the MLE is above 0, the time trace is deemed to be a chaos. The MLEs calculated for different waveforms at the different bias voltages is given in Fig. 9. When a bias voltage is lower than 3.95 V, the corresponding MLE is smaller than zero. While a voltage is between 3.96 V and 4.6 V, the MLE is bigger than zero and the RC system is in the chaotic state. The bias voltage at 3.95 V is the critical value where the transient state between the period oscillation and chaos appears.

The identification at the different bias voltages is shown in Fig. 10. As can be seen, the optimal bias voltage is 3.95 V where the minimal NRMSE is 0.2283 and the minimal WER is 1.25%, i.e., 79 among 80 optical headers can be identified correctly.

In our experiment, to adjust the attenuation of VOA3 is equivalent to adjust the feedback coefficient β. Fig. 11 shows the recognition results whose NRMSE curve is V-shaped. We can obtain the optimal feedback optical power is -1.2 dBm with the minimal NRMSE of 0.2283 and the minimal WER of 1.25%. Yet curves in Figs. 3 and 11 are similar in V-shaped trend. Therefore, the optimal feedback light power as -1.2 dBm is consistent with the optimal feedback coefficient β as 2. For these values the optoelectronic feedback reservoir computing is in the transient state to provide the optimal recognition results. Fig. 11 gives the recognition results whose NRMSE curve is V-shaped. We can

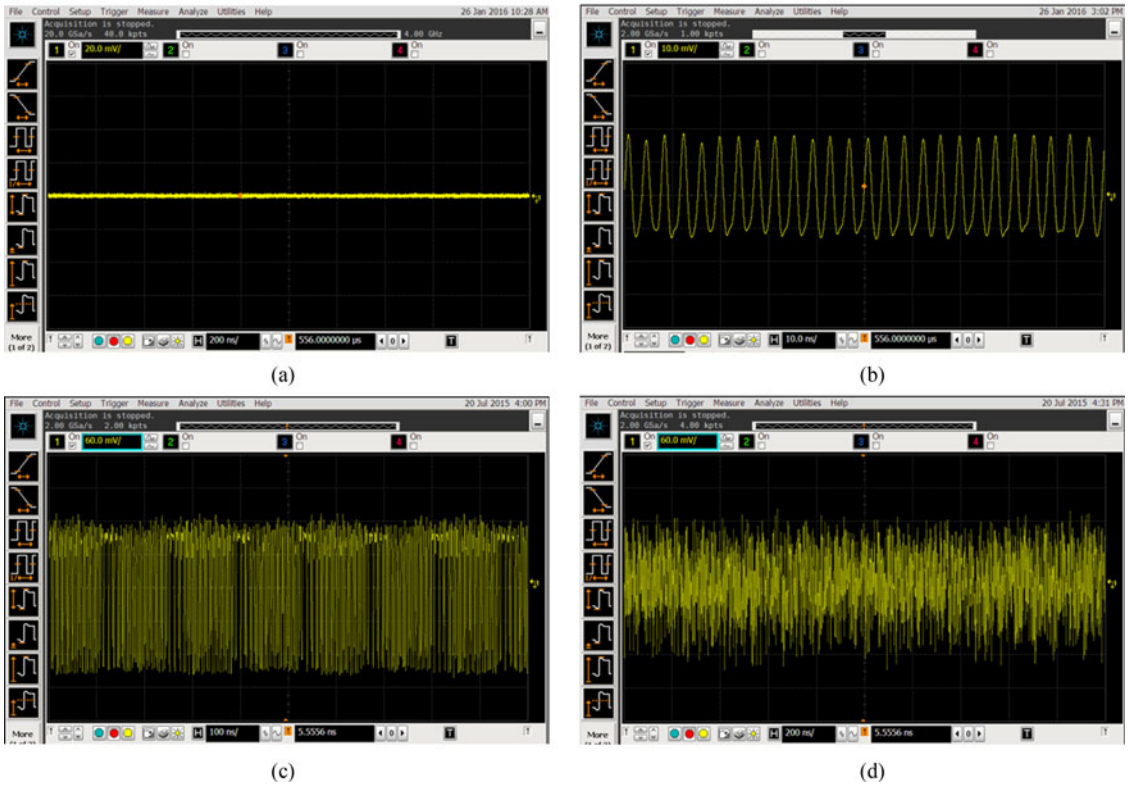

Fig. 8. Different waveforms observed on the oscilloscope under different bias voltages with (a) Vbias = 0 V, (b) Vbias = 3 V, (c) Vbias = 3.9 V, and (d) Vbias = 4.1 V.

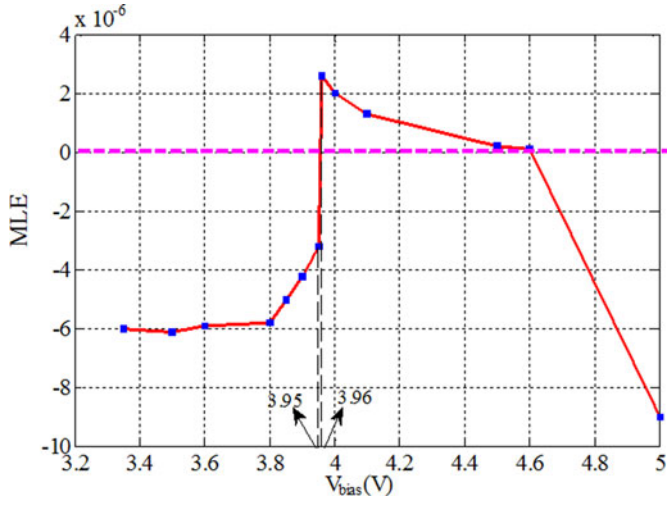

Fig. 9. Maximal Lyapunov exponents for the different bias voltages.

get the optimal feedback optical power is −1.2 dBm with the minimal NRMSE of 0.2283 and the minimal WER of 1.25%.

As mentioned above, the optimal parameters are as follows: the MZM bias voltage V_{bias} is 3.95 V and the optimal feedback optical power is −1.2 dBm for our optoelectronic feedback RC system. The graph of desired recognition results and actual recognition results are shown in Fig. 12(i) and (ii), respectively. The warm color bars at the vertical axis indicate the clustering result. If the actual

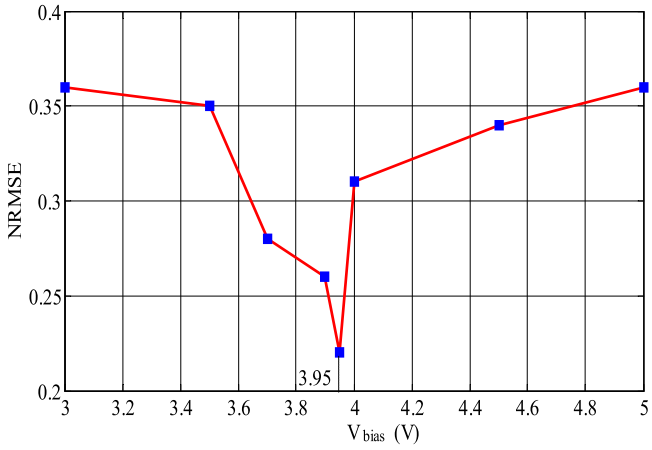

Fig. 10. NRMSE of the identification at different bias voltages.

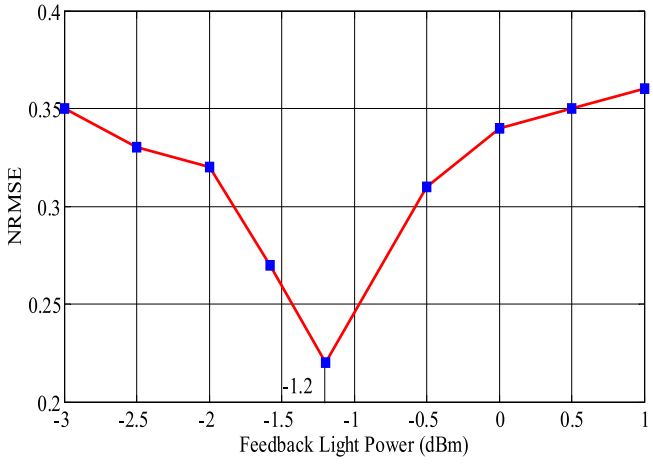

Fig. 11. NRMSE of the identification under the different feedback optical power.

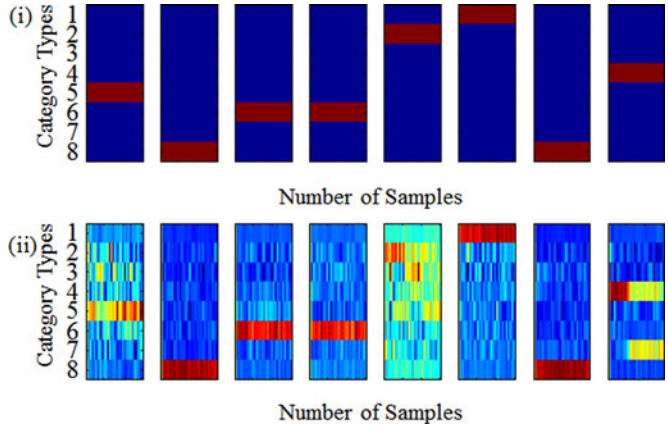

Fig. 12. Identification results of the 3 bits optical packet header for the optimal parameters. (i) Desired outputs, (ii) actual outputs.

output is closer to the desired output, the lower subgraph is more similar to the upper subgraph. Fig. 12(i) and (ii) indicate the good similarity corresponding to the minimal NRMSE of 0.2283 and the minimal WER of 1.25% for the 3-bit optical header identification.

5. Conclusion

In this paper, an optoelectronic feedback reservoir computing system that can identify the optical packet headers is proposed and investigated by both numerical simulation and physical implementation. We simulate the recognition of the optical packet headers whose lengths are from 3 bits to 32 bits, respectively. In the simulation, we optimized the system parameters such as the feedback coefficient and the SNR to get the minimal NRMSE below 0.04 and the minimal WER as 0. The experiment verifies the feasibility of the optical packet header recognition based on the optoelectronic feedback RC and indicates the optimal parameters as the bias voltage and the feedback optical power. The proposed recognition system has many advantages such as the simple structure, the easy realization and the good noise tolerance. It can be employed for the high-speed optical packet header processing and other important applications in the future OPS network.

References

[1] M. J. O'Mahony, D. Simeonidou, D. K. Hunter, and A. Tzanakaki, "The application of optical packet switching in future communication networks," *IEEE Commun. Mag.*, vol. 39, no. 3, pp. 128–135, Mar. 2001.

[2] N. Calabretta, H. D. Jung, E. Tangdiongga, and H. Dorren, "All-optical packet switching and label rewriting for data packets beyond 160 Gb/s," *IEEE Photon. J.*, vol. 2, no. 2, pp. 113–129, Apr. 2010.

[3] S. A. Nezamalhosseini, M. R. Dizaji, K. Fouli, L. R. Chen, and F. Marvasti, "Novel FWM-based spectral amplitude code label recognition for optical packet-switched networks," *IEEE Photon. J.*, vol. 5, no. 4, Aug. 2013, Art. no. 6601510.

[4] M. C. Cardakli, S. Lee, A. E. Willner, V. Grubsky, D. Starodubov, and J. Feinberg, "Reconfigurable optical packet header recognition and routing using time-to-wavelength mapping and tunable fiber Bragg gratings for correlation decoding," *IEEE Photon. Technol. Lett.*, vol. 12, no. 5, pp. 552–554, May 2000.

[5] M. T. Hill *et al.*, "1 $\times$ 2 optical packet switch using all-optical header processing," *Electron. Lett.*, vol. 37, no. 12, pp. 774–775, 2001.

[6] J. M. Martinez, F. Ramos, and J. Marti, "All-optical packet header processor based on cascaded SOA-MZIs," *Electron. Lett.*, vol. 40, no. 14, pp. 894–895, 2004.

[7] K. Okubo, H. Kishikawa, N. Goto, and S. I. Yanagiya, "Optical QPSK label recognition by time-space conversion using two-dimensional matched filtering," *J. Commun. Comput.*, vol. 10, pp. 214–219, 2013.

[8] K. Mizote, H. Kishikawa, N. Goto, and S. I. Yanagiya, "Optical label routing processing for BPSK labels using complex-valued neural network," *J. Lightw. Technol.*, vol. 31, no. 12, pp. 1867–1876, Jun. 2013.

[9] K. Mizote, H. Kishikawa, N. Goto, and S. I. Yanagiya, "All-optical label processing using complex-valued neural network learned with back propagation of teacher signals," in *Proc. 16th Opto-Electron. Commun. Conf.*, Jul. 2011, pp. 275–276.

[10] T. Mizobuchi, K. Mizote, H. Kishikawa, N. Goto, and S. I. Yanagiya, "QPSK label processing using complex-valued neural network learned with back propagation of teacher signals," in *Proc. 17th Opto-Electron. Commun. Conf.*, 2012, pp. 309–310.

[11] C. Mesaritakis, A. Kapsalis, and D. Syvridis, "All-optical reservoir computing system based on In GaAsP ring resonators for high-speed identification and optical routing in optical networks," in *Proc. SPIE OPTO Int. Soc. Opt. Photon.*, Feb. 2015, pp. 937033.

[12] M. Hermans, M. C. Soriano, J. Dambre, P. Bienstman, and I. Fischer, "Photonic delay systems as machine learning implementations," *J. Mach. Learn. Res.*, vol. 16, pp. 2081–2097, 2015.

[13] F. Duport, B. Schneider, A. Smerieri, M. Haelterman, and S. Massar, "All-optical reservoir computing," *Opt. Exp.*, vol. 2, no. 20, pp. 22783–22795, 2012.

[14] A. Dejonckheere *et al.*, "All-optical reservoir computer based on saturation of absorption," *Opt. Exp.*, vol. 22, no. 9, pp. 10868–10881, 2014.

[15] L. Appeltant *et al.*, "Information processing using a single dynamical node as complex system," *Nature Commun.*, vol. 2, 2011, Art. no. 468.

[16] S. Ortín *et al.*, "A unified framework for reservoir computing and extreme learning machines based on a single time-delayed neuron," *Sci. Rep.*, vol. 5, 2015, Art. no. 14945.

[17] L. Larger *et al.*, "Photonic information processing beyond Turing: an optoelectronic implementation of reservoir computing," *Opt. Exp.*, vol. 20, no. 3, pp. 3241–3249, 2012.

[18] Y. Paquot *et al.*, "Optoelectronic reservoir computing," *Sci. Rep.*, vol. 2, 2012, Art. no. 287.

[19] Y. Jin, Q. Zhao, H. Yin, and H. Yue, "Handwritten numeral recognition utilizing reservoir computing subject to optoelectronic feedback," in *Proc. IEEE 11th Int. Conf. Natural Comput.*, Aug. 2015, pp. 1165–1169.

[20] F. Duport, A. Smerieri, A. Akrout, M. Haelterman, and S. Massar, "Virtualization of a photonic reservoir computer," *J. Lightw. Technol.*, vol. 34, no. 9, pp. 2085–2091, May 2016.

[21] C. Mesaritakis, A. Bogris, A. Kapsalis, and D. Syvridis, "High-speed all-optical pattern recognition of dispersive Fourier images through a photonic reservoir computing subsystem," *Opt. Lett.*, vol. 40, no. 14, pp. 3416–3419, 2015.

[22] J. Qin, Q. Zhao, D. Xu, H. Yin, Y. Chang, and D. Huang, "Optical packet header identification utilizing an all-optical feedback chaotic reservoir computing," *Mod. Phys. Lett. B*, vol. 30, 2016, Art. no. 1650199.
[23] F. Duport, A. Smerieri, A. Akrout, M. Haelterman, and S. Massar, "Fully analogue photonic reservoir computer," *Sci. Rep.*, vol. 6, 2016, Art. no. 22381.
[24] J. Nakayama, K. Kanno, and A. Uchida, "Laser dynamical reservoir computing with consistency: An approach of a chaos mask signal," *Opt. Exp.*, vol. 24, no. 8, pp.8679–8692, 2016.
[25] I. Fischer, J. Bueno, D. Brunner, M. C. Soriano, and C. Mirasso, "Photonic Reservoir computing for ultra-fast information processing using semiconductor lasers," in *Proc. 42nd Eur. Conf. Opt. Commun.*, Dec. 2016, pp. 1–3.
[26] R. M. Nguimdo, G. Verschaffelt, J. Danckaert, and G. Van der Sande, "Fast photonic information processing using semiconductor lasers with delayed optical feedback: Role of phase dynamics," *Opt. Exp.*, vol. 22, no. 7, pp. 8672–8686, 2014.
[27] R. M. Nguimdo, G. Verschaffelt, J. Danckaert, and G. Van der Sande, "Simultaneous computation of two independent tasks using reservoir computing based on a single photonic nonlinear node with optical feedback," *IEEE Trans. Neural Netw. Learn. Syst.*, vol. 26, no. 12, pp. 3301–3307, Dec. 2015.
[28] C. Mesaritakis, V. Papataxiarhis, and D. Syvridis, "Micro ring resonators as building blocks for an all-optical high-speed reservoir-computing bit-pattern-recognition system," *JOSA B*, vol. 30, no. 11, pp. 3048–3055, 2013.
[29] M. Bauduin, T. Deleu, F. Duport, P. De Doncker, S. Massar, and F. Horlin, "Equalization of the non-linear 60 GHz channel: Comparison of reservoir computing to traditional approach," in *Proc. IEEE Werkgemeenschap voor Informatie-en Communicatietheorie Symp.*, May 2013, pp. 1–8.
[30] R. M. Nguimdo, G. Verschaffelt, J. Danckaert, and G. Van der Sande, "Reducing the phase sensitivity of laser-based optical reservoir computing systems," *Opt. Exp.*, vol. 24, no. 2, pp. 1238–1252, 2016.
[31] A. E. Hoerl and R. W. Kennard, "Ridge regression: Biased estimation for nonorthogonal problems," *Technometrics*, vol. 12, no. 1, pp. 55–67, 1970.
[32] A. F. Atiya and A. G. Parlos, "New results on recurrent network training: Unifying the algorithms and accelerating convergence," *IEEE Trans. Neural Netw.*, vol. 11, no. 3, pp. 697–709, May 2000.
[33] L. Larger and J. M. Dudley, "Nonlinear dynamics: Optoelectronic chaos," *Nature*, vol. 465, no. 7294, pp. 41–42, 2010.
[34] K. E. Callan, L. Illing, Z. Gao, D. J. Gauthier, and E. Schöll, "Broadband chaos generated by an optoelectronic oscillator," *Phys. Rev. Lett.*, vol. 104, no. 11, 2010, Art. no. 113901.
[35] M. C. Soriano *et al.*, "Delay-based reservoir computing: noise effects in a combined analog and digital implementation," *IEEE Trans. Neural Netw. Learn. Syst.*, vol. 26, no. 2, pp. 388–393, Feb. 2015.
[36] M. C. Soriano *et al.*, "Optoelectronic reservoir computing: tackling noise-induced performance degradation," *Opt. Exp.*, vol. 21, no. 1, pp. 12–20, 2013.
[37] H. Han and K. A. Shore, "Dynamics and stability of mutually coupled nano-lasers," *IEEE J. Quantum Electron.*, vol. 52, no. 11, pp. 1–6, Nov. 2016.
[38] T. Zhao *et al.*, "Precise fault location in TDM-PON by utilizing chaotic laser subject to optical feedback," *IEEE Photon. J.*, vol. 7, no. 6, pp. 1–9, Dec. 2015.
[39] A. Wang, B. Wang, L. Li, Y. Wang, and K. A. Shore, "Optical heterodyne generation of high-dimensional and broadband white chaos," *IEEE J. Sel. Topics Quantum Electron.*, vol. 21, no. 6, pp. 531–540, Nov./Dec. 2015.
[40] L. X. Wang, N. H. Zhu, J. Y. Zheng, J. G. Liu, and W. Li, "Chaotic ultra-wideband radio generator based on an optoelectronic oscillator with a built-in microwave photonic filter," *Appl. Opt.*, vol. 51, no. 15, pp. 2935–2940, 2012.
[41] R. Rahamim, U. Mahlab, and D. Dahan, "Identification of linear and nonlinear propagation regimes in an optical fiber link using chaos analysis," *Opt. Eng.*, vol. 48, no. 10, Oct. 2009, Art. no. 105002.
[42] Q. Fan, H. Li, and H. Yin, "Study on optical performance monitoring for fiber-optical link utilizing chaos theory," *Adv. Mater. Res.*, vol. 571, pp. 390–394, 2012.
[43] Q. Fan, H. Yin, W. Chang, Q. Zhao, and N. Zhao, "Experimental investigation on identification of physical defect of WDM optical-fiber links based on chaos theory, " in *Proc. Conf. Lasers Electro-Opt.*, 2013, Paper JTu4A.93.